HCN fluorescence on Titan

Roger V. Yelle [*] and Caitlin A. Griffith

Department of Planetary Science and Lunar and Planetary Laboratory, University of Arizona, Tucson, AZ 85721, USA

Received 10 February 2003; revised 15 May 2003

Abstract

The HCN emission features near 3 μm recently detected by Geballe et al. (2003, Astrophys. J. 583, L39) are analyzed with a model for fluorescence of sunlight in the ν_3 band of HCN. The emission spectrum is consistent with current knowledge of the atmospheric temperature profile and the HCN distribution inferred from millimeter-wave observations. The spectrum is insensitive to the abundance of HCN in the thermosphere and the thousand-fold enhancement relative to photochemical models suggested by Geballe et al. (2003, Astrophys. J. 583, L39) is not required to explain the observations. We find that the spectrum can be matched with temperatures from 130 to 200 K, with slightly better fits at high temperature, contrary to the temperature determination of 130 ± 10 K of Geballe et al. (2003, Astrophys. J. 583, L39). The HCN emission spectrum is sensitive to the collisional de-excitation probability, P_{10}, for the ν_3 state and we determine a value of 10^{-5} with an accuracy of about a factor of two. Analysis of absorption lines in the C_2H_2 ν_3 band near 3 μm, detected in the same spectrum, indicate a C_2H_2 mole fraction near 0.01 μbar of 10^{-5} for $P_{10} = 10^{-4}$. The derived mole fraction, however, is dependent upon the value adopted for P_{10} and lower values are required if P_{10} at Titan temperatures is less than its room temperature value.
© 2003 Elsevier Inc. All rights reserved.

Keywords: Titan; Atmosphere; Composition; Temperature

1. Introduction

Recently, Geballe et al. (2003) discovered HCN emissions from Titan along with C_2H_2 absorption lines in a high resolution spectrum of the region near 3 μm. Geballe et al. (2003) show that the emissions are due to fluorescence of sunlight in the C–H stretch, ν_3 band of HCN. Previously, fluorescence in the ν_3 band of CH_4, which is also a C–H stretch mode, has been detected on Titan and Jupiter (Kim et al., 1996, 2000; Dinelli et al., 1997; Drossart et al., 1998) and in cometary comae (Weaver et al., 1989). Geballe et al. (2003) show that the emission features can be used to probe atmospheric structure and derived a rotational temperature of 130 ± 10 K and an HCN mole fraction of 0.3–1.0% near Titan's mesopause from analysis of the spectrum. The temperature is close to the predicted values (Yelle, 1991) but Geballe et al. (2003) claim that the HCN mole fraction is roughly three orders of magnitude larger than predicted by chemical models of the atmosphere. The temperature and HCN abundance in Titan's upper atmosphere are closely coupled and a large increase in the HCN mole frac-

tion should be accompanied by a decrease in temperature (Yelle, 1991). In addition, the C_2H_2 spectral lines are seen in absorption, which is surprising considering that the strengths of the C_2H_2 and HCN bands are nearly identical (Geballe et al., 2003). We therefore present below a more comprehensive analysis of these spectral features.

Fluorescent emissions from planetary atmospheres occur when excited molecular energy levels undergo radiative transitions to a lower level. Strong emission lines can be formed if the radiative de-excitation rate, A_{10} is larger than the collisional de-excitation, C_{10}. Collisional de-excitation rates are proportional to atmospheric density and the ratio A_{10}/C_{10} determines the formation region for emission lines. An important aspect of fluorescence in vibrational bands is that collisional de-excitation of vibrational states is slow (typically 10^4–10^5 collisions are required to cause a downward transition (Lambert, 1977) and radiative de-excitation tends to dominate in the upper atmosphere. If the collisional de-excitation rates are known, this circumstance can be exploited to interpret the intensity of emission lines in terms of the density of the fluorescent species above the altitude where $A_{10} \sim C_{10}$. On the other hand, collisional redistribution of rotational states is rapid and tends to dominate at all altitudes. Collisions force an equilibration between rota-

* Corresponding author.
E-mail address: yelle@lpl.arizona.edu (R.V. Yelle).

tional and translational modes so the rotational populations of each vibrational state follow a Boltzmann distribution at the local atmospheric temperature, even if the vibrational populations themselves do not. This implies that relative rotational line intensities are sensitive to the atmospheric temperature, though proper account must be taken of radiative transfer in the band to interpret the spectrum in terms of temperature.

2. Model description

The HCN emission lines are produced by emission from the ν_3 level excited from the ground state by the absorption of a solar photon (Geballe et al., 2003). Thermal excitation due to collisions with ambient molecules is ~ 5 orders of magnitude smaller than solar excitation. In principle ν_3 excitation may also be caused by absorption of solar photons into higher energy ν_3 overtone states, which then cascade downward to the ν_3 level. However, this process would produce $2\nu_3 \rightarrow \nu_3$ spectral features, which are not observed. Calculation of the solar energy deposition rate in the $2\nu_3$ band reveal that, because it is roughly two orders of magnitude weaker than the ν_3 band, photons are absorbed primarily in the lower stratosphere, where large collisional de-excitation rates prevent any significant fluorescence. We can therefore rule out observationally and theoretically the possibility of a significant cascade contribution.

The HCN fluorescence spectrum depends upon the relative radiative and collisional decay rates, the atmospheric temperature profile, and the altitude distribution of HCN. Listed in Table 1 are radiative decay rates for the ν_3 bands of HCN and C_2H_2 along with the collisional de-excitation rate constant as measured at room temperature. The collisional de-excitation rate is equal to the product of the rate constant and atmospheric density $C_{10} = k_{10}N_\circ$. Setting $C_{10} = A_{10}$ and assuming a temperature of 175 K, we find that the collisional and radiative de-excitation rates are equal at ~ 0.1 mbar. However, collisional de-excitation rates are expected to decrease with decreasing temperature and the values of k_{10} measured in the laboratory should be larger than the values that apply to Titan. Thus the HCN emissions should probe Titan's atmosphere to at least the 0.1 mbar level and possibly deeper.

The collisional de-excitation rates C_{10} can be written as

$$C_{10} = P_{10}\pi\sigma^2 N_\circ \sqrt{8kT/\pi m}, \qquad (1)$$

Table 1
Band parameters

	HCN	C_2H_2
ν_{10} (cm^{-1})	3314	3300
A_{10} (Hz)	86	85
k_{10}[a] (cm^2 s^{-1})	2.6×10^{-14}	3.1×10^{-14}
P_{10}[a]	9.7×10^{-5}	9×10^{-5}

[a] Values at 296 K.

where σ is the diameter for collisions, assumed to be 4 Å, $\sqrt{8kT/\pi m}$ is the mean velocity of collisions, and P_{10} is the probability that a collision induces a transition out of the vibrationally excited state. The primary uncertainty in C_{10} is due to P_{10}. Hastings et al. (1983) have measured $P_{10} = 9.7 \times 10^{-5}$ for HCN-N$_2$ collisions at room temperature. They argue that de-excitation occurs through a V–V transition to the $\nu_1 + \nu_2$ state, rather than directly to the ground state even though the reaction is endothermic by $\Delta E \sim 200$ cm^{-1}. This is reasonable because the energy difference is roughly equal to thermal energy (kT) at 296 K, but it suggests that the rate could be highly temperature sensitive. In fact, low temperature de-excitation probabilities are usually significantly lower than their room temperature values (Yelle, 1991). We show later that a value of $P_{10} = 10^{-5}$, a factor of 10 lower than the room temperature measurements, provides a good fit to the HCN emission lines in the observed spectrum. We note that the rate constant adopted by Geballe et al. (2003) is equivalent to $P_{10} = 0.04$, and is much higher than the experimental value.

The collision de-excitation probability for the ν_3 band of C_2H_2 has been measured by Hager et al. (1980). These authors find $P_{10} = 9 \times 10^{-5}$ for collisions with N$_2$ at room temperature, approximately equal to the value for HCN. As with HCN, de-excitation is believed to occur through V–V transfer to a complex combination band that is easily de-excited. For C_2H_2, however, the nearby vibrational complex is at approximately the same energy as the ν_3 band so the rate should be less temperature sensitive than it is for HCN. We adopt $P_{10} = 10^{-4}$ for C_2H_2 for our baseline model.

The altitude profile of HCN in Titan's stratosphere is well established from millimeter wave observations (Marten et al., 2002). The disc-averaged mole fraction increases slowly with altitude from a value of 4×10^{-8} at 10 mbar to 8×10^{-7} at 4 µbar. At altitudes below 10 mbar HCN condenses and its mole fraction drops rapidly to zero. At altitudes above 4 µbar, photochemical models predict a mole fraction in the thermosphere, X_∞(HCN), of $\sim 3 \times 10^{-3}$ (Yung et al., 1984). According to Yung et al. (1984) the large values of HCN are reached at a pressure of $\sim 10^{-3}$ µbar. We interpolate between the Marten et al. (2002) results at 4 µbar and $X_\infty = 3 \times 10^{-3}$ at 10^{-3} µbar by assuming that the mole fraction varies linearly with log pressure. This procedure yields an HCN mole fraction of 2.5×10^{-4} at 600 km, a factor of ~ 30 smaller than the value suggested by Geballe et al. (2003). We also consider models with X_∞ equal to 10^{-4} and 10^{-6}.

There is less information on the altitude profile of C_2H_2. Analysis of Voyager IRIS observations yields mole fraction of $3.0 \pm 0.3 \times 10^{-6}$ in the equatorial stratosphere (Coustenis et al., 1995), increasing to $6.6 \pm 2.1 \times 10^{-6}$ at 70° N, whereas analysis of disc averaged observations by ISO (Coustenis et al., 2003) determines a mole fraction of 4.5×10^{-6} near 1 mbar. Photochemical models predict that the C_2H_2 mole fraction increases to values of $\sim 10^{-3}$ in the thermosphere (Yung et al., 1984; Toublanc et al., 1995; Lara
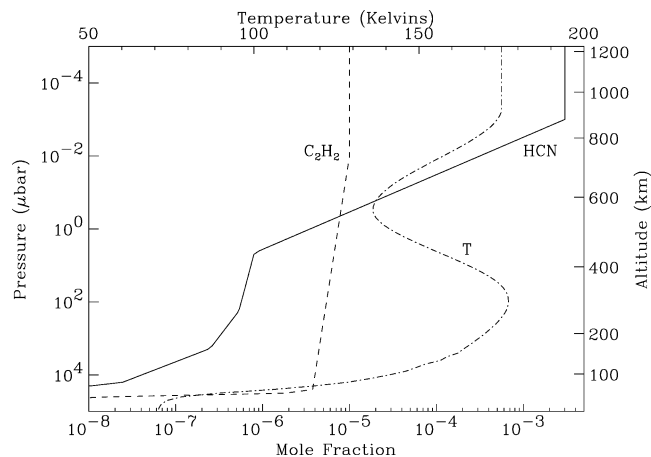
Fig. 1. The altitude distributions of HCN, C_2H_2 and temperature used in the baseline model atmosphere.

et al., 1996); however, an abundance this large is inconsistent with Voyager UVS occultation results (Vervack, 1997). Our baseline model has a C_2H_2 mole fraction in the thermosphere of $X_\infty = 10^{-5}$. We connect the stratospheric mole fractions to that adopted for the thermosphere by assuming that the thermospheric abundance applies to 0.01 µbar and that the mole fraction varies linearly as log pressure between 10 mbar and 0.01 µbar. Condensation of C_2H_2 is included at deeper levels. The baseline model atmosphere is shown in Fig. 1.

We use the temperature profile of Yelle et al. (1997) in our analysis, which is constructed to satisfy a variety of constraints from observations and models. Temperatures at pressures greater than 1 mbar have been determined through a combination of radio occultation measurements (Lindal et al., 1983) and measurements of the CH_4 band at 7.8 µm (Coustenis et al., 1995, 2003). Temperatures in the thermosphere have been determined through UV occultation (Smith et al., 1983). The region near 1 µbar is expected both theoretically and observationally to have a negative temperature gradient. Observational evidence comes from comparison of densities at higher and lower altitudes which, through hydrostatic equilibrium, determine a mean temperature less than the values at higher and lower altitudes (Lellouch et al., 1990). Theoretical evidence comes from thermal structure models that predict a well developed mesopause near 0.1 µbar (Yelle, 1991). Yelle et al. (1997) also presents maximum and minimum temperature models, but these are designed for spacecraft engineering use and are extremely conservative. Examination of the uncertainties in the observations and models suggest that 5 K is a more reasonable value for the temperature uncertainty near 1 mbar at the time of the observations (Coustenis et al., 2003).

3. Spectral calculation

We synthesize the near IR spectrum of Titan by solving the radiative transfer equation for overlapping vibrational bands in rotational LTE. To implement the radiative transfer equations we use a vertical grid that extends from 10^5 to 10^{-4} µbar and is sampled at a rate of 10 levels per decade of pressure. Both HCN and C_2H_2 lines are included in the calculation and are treated in an identical manner. Line parameters are obtained from the GEISA database (Jacquinet-Husson et al., 1999). The spectrum is calculated in vacuum wavenumbers at a resolution of 0.003 cm^{-1} then converted to air wavelengths and smoothed to a resolving power of 20,000 for comparison with the observations. The coupled radiative transfer equations for the two bands are solved with a modified Rybicki technique using six angular streams. The formulation of the radiative transfer equation and the numerical technique used in its solution are described in Appendix A. The solar incidence and emission angles are set to 60 degrees to simulate a disc-averaged spectrum. The continuum level seen in the observations is established by scattering of sunlight by aerosols and absorption by the far wings of pressure-broadened CH_4 lines in the lower stratosphere and troposphere (Griffith et al., 1998). Because the continuum is established at pressures greater than those of interest here, we do not treat it rigorously but instead model the effect of aerosol scattering and CH_4 absorption by specifying a Lambertian reflecting surface at the lower boundary whose frequency dependent albedo is adjusted to reproduce the observed continuum levels.

Results for the baseline model are compared with the observations in Fig. 2, where we show only the P branch. There are significant differences between the line intensities in the R and P branches which Geballe et al. (2003) suggest are due to difference in pointing because the R and P branches were measured in different exposures. We follow Geballe et al. (2003) and analyze only the P branch. The spectrum also has gaps due to difficulty in correcting for telluric absorption features (Geballe et al., 2003) and, in particular, the P(1), P(9), and P(15) lines are missing, presumably because of this problem. Aside from these spectral gaps, the emission spectrum is well matched by the model. Most absorption and emission lines are fit to within $\pm 2 \times 10^{-15}$ W m^{-2} µm^{-1} and the C_2H_2 absorption features are about as well matched as the HCN emission lines.

Examination of the radiative transfer source function reveals several characteristics of HCN line formation. Figure 3 shows the direct solar source function, the multiply scattered source function and the net source function for the HCN and C_2H_2 bands. These quantities are precisely defined in Appendix A. At high altitudes the direct solar contribution to the source functions, S°, dominates, but the scattering contribution, J, is everywhere significant and for HCN becomes larger than S° at pressures greater than ~ 50 µbar. Scattering is less important for C_2H_2, but even for this band J is $\sim 40\%$ of S°. The decrease of S° with increasing pressure for HCN indicates that the lines are optically thick, contrary to assertions in Geballe et al. (2003). The optically thin approximation does appear adequate for C_2H_2 for our baseline model. The strength of the scattering term and the importance of op-
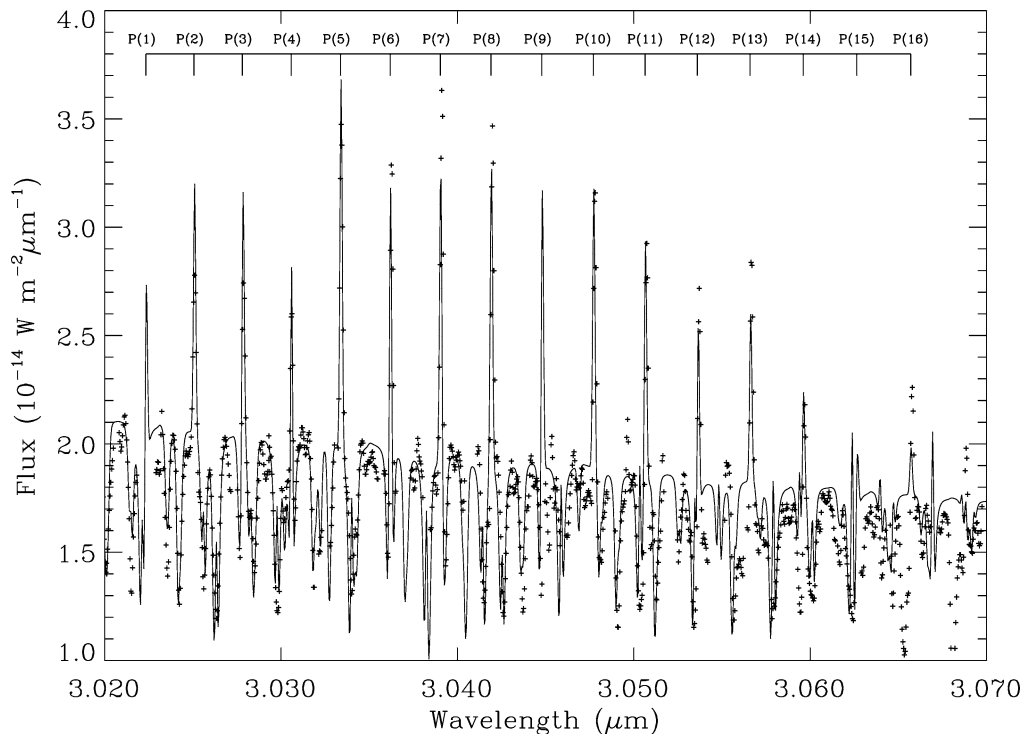
Fig. 2. Observations and baseline model for the spectral region containing the HCN P branch. Note that the P(1), P(9), and P(15) line are not observed as a result of telluric absorption. The data are from Geballe et al. (2003).
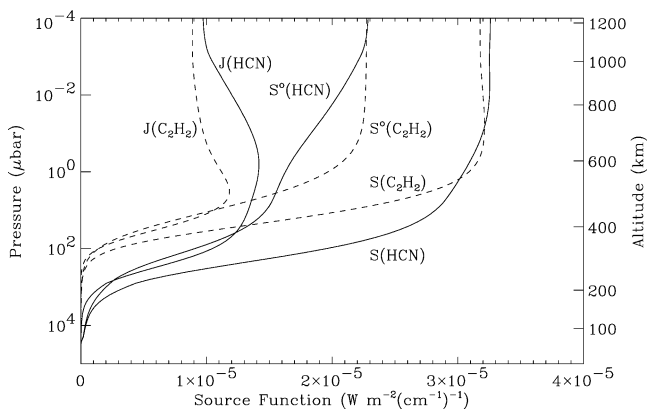
Fig. 3. The direct solar source function $S°$, the multiply scattered source function J, and the net source function, S for the HCN and C_2H_2 bands.

Fig. 4. A high resolution synthetic spectrum showing details of the HCN and C_2H_2 line profiles.

tical depth demonstrate that full scattering calculations are necessary to accurately calculate the intensity in the HCN band. The HCN source function falls to zero near 1 mbar and the C_2H_2 source function near 100 μbar because the single scattering albedo becomes significantly less than unity and the atmosphere becomes absorptive rather than scattering. This aspect of the problem is discussed in more detail below.

The HCN and C_2H_2 source functions are similar, yet the HCN lines appear in emission and the C_2H_2 lines in absorption. The solution to this puzzle becomes apparent when the spectrum is examined at high resolution. Figure 4 shows a synthetic spectrum for a small region containing both an

HCN and C_2H_2 line, at a resolution approximately equal to the Doppler width of the lines. The C_2H_2 line consists of a strong emission feature near line center sitting in a deep absorption feature that extends to the wings of the line. These two aspects of the line profile are smoothed together at the resolution of the observations and the net effect is an absorption line that is less deep than it would be in the absence of fluorescence. The HCN line also has an emission feature near line center and absorption in the wings, but the absorption is significantly weaker than for C_2H_2 and the HCN lines appear in emission. The different strengths of absorption portions of the HCN and C_2H_2 lines are a consequence of the
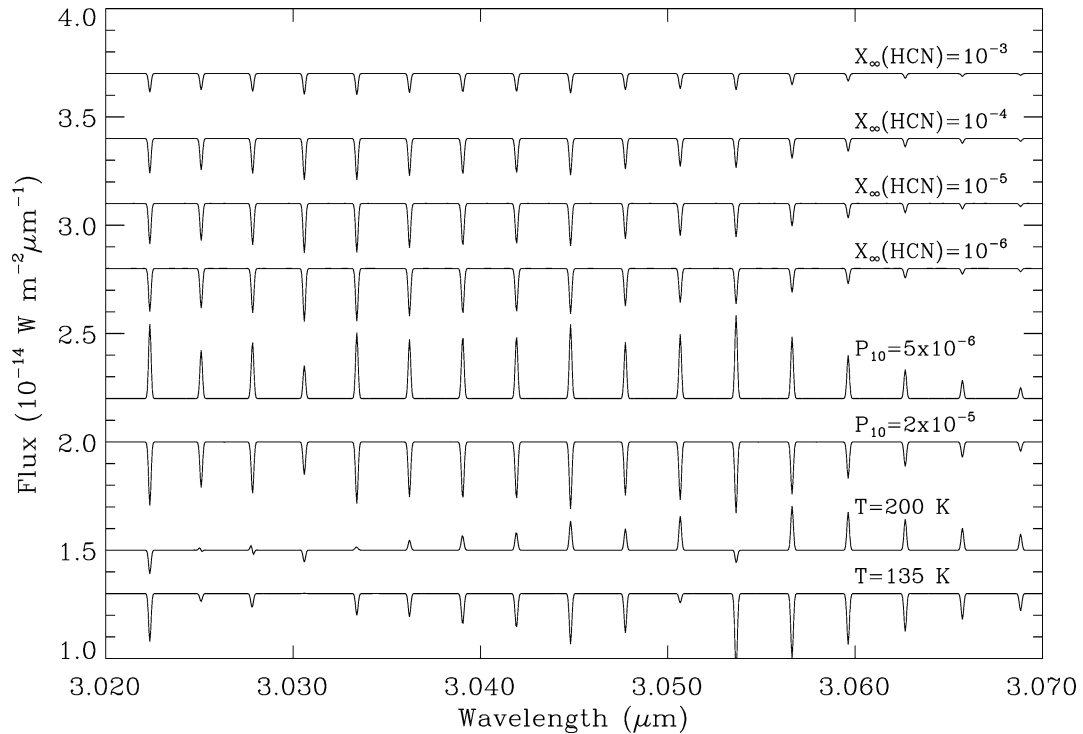
Fig. 5. Sensitivity tests for HCN model parameters. The curves show the difference between the modified models and the baseline model. Only one parameter is modified at a time and the varied parameter is listed next to the curve.

different altitude distribution of these species. As shown in Fig. 1, C_2H_2 is more abundant than HCN in the stratosphere, where the absorptive wings of the line profile are formed. Partly this is a consequence of photochemistry and partly reflects the lower vapor pressure of HCN. As a result, absorption dominates for C_2H_2 and fluorescence for HCN.

4. Sensitivity tests

We have calculated a number of model HCN spectra to determine the effects of X_∞, P_{10}, and the temperature profile. In Fig. 5 we show the difference between models with modified parameters and the baseline model. We vary parameters until the difference between the modified model and the baseline model is $\sim 2 \times 10^{-15}$ W m^{-2} µm^{-1}, which is also approximately the accuracy of the fit between baseline model and the observations. The effect of varying X_∞ is surprisingly small. The differences only reach 2×10^{-15} W m^{-2} µm^{-1} for $X_\infty = 10^{-6}$. The reason for this is presented in Fig. 6, which shows the solar flux absorbed in the HCN band as a function of pressure along with the single scattering albedo for the band, ϖ. Roughly speaking, HCN above the $\varpi = 0.5$ level scatters solar photons, forming the emission part of the line profile, while HCN below the $\varpi = 0.5$ level forms the absorption part of the line profile. Figure 6 shows that for $P_{10} = 10^{-5}$ the flux scattered in the band is essentially independent of X_∞. This is because the scattering column extends to ~ 1 mbar for $P_{10} = 10^{-5}$ and the contribution from HCN above 10^{-3} µbar is insignificant.
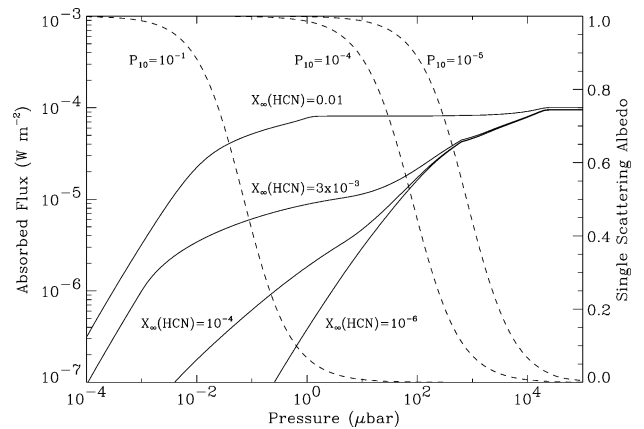
Fig. 6. The solid lines show solar flux absorbed in the HCN and C_2H_2 bands and the dashed lines the single scattering albedo for the bands. Model parameters are listed next to the curves. Parameters not shown are equal to those in the baseline model. The curves show the interplay between X_∞ and P_{10}. For example, the same solar flux is absorbed above the $\varpi = 0.65$ level in the models with $X_\infty(\text{HCN}) = 3 \times 10^{-3}$ and $P_{10} = 10^{-5}$, and $X_\infty(\text{HCN}) = 0.01$, and $P_{10} = 0.1$.

The HCN abundance from the lower stratosphere to 4 µbar has been determined from analysis of millimeter-wave observations (Marten et al., 2002). Assuming these values, we can determine P_{10}.

The strength of the HCN emission lines is more sensitive to P_{10}. A value of $P_{10} = 2 \times 10^{-5}$, twice as large as that used in the baseline model, produces a poor fit to the observed spectrum. The explanation is again shown in Fig. 6. The absorbed flux increases rapidly with pressure in
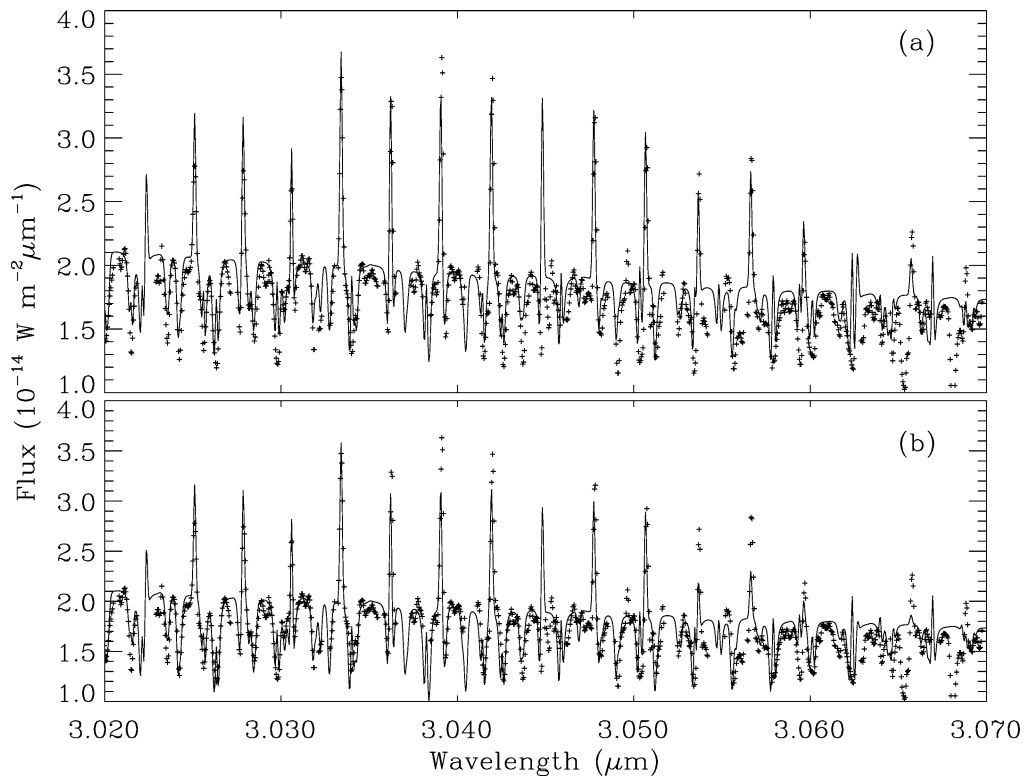
Fig. 7. (a) Comparison of model and observations using a temperature of 200 K to calculate the HCN line parameters. (b) Calculations using a temperature of 135 K to calculate the HCN line parameters.

the 10^2–10^3 μbar region and by varying P_{10} we are altering significantly the solar flux absorbed in the scattering region of the atmosphere. Similarly a value of $P_{10} = 5 \times 10^{-6}$ produces emission lines that are too bright. We conclude that $P_{10} = 10^{-5}$ at Titan temperatures, with an uncertainty of a factor of two.

The HCN emission lines are weakly sensitive to temperature. To examine this aspect of the problem we specify in the calculations a constant temperature which is used only to calculate HCN line strengths and widths; the rest of the model atmosphere and the C_2H_2 emission lines remain unchanged. We show results in Figs. 7a and 7b. A temperature of 135 K produces weaker high J lines than the nominal temperature profile, by an amount that is marginally significant. The variation, however, is in a direction that degrades the fit to the observed spectrum. A temperature of 200 K also produces changes to the spectrum of marginal significance, although these are in the direction that would improve the fit to the observations. Based on the previous discussion, HCN line strengths should be determined primarily by the temperature near 1 mbar. This may indicate that temperatures in this region are higher than assumed in our baseline model. In fact, a recent analysis of ISO observations of Titan (Coustenis et al., 2003) retrieves temperatures near 1 mbar ∼ 5 K warmer than we assume. This suggests that the HCN emissions may be a useful probe of temperature in Titan's atmosphere, but higher quality observations are needed.

Geballe et al. (2003) argued that a rotational temperature of 130 ± 10 K could be inferred from the HCN spectrum. This led them to adopt a collisional de-excitation rate equivalent to $P_{10} = 0.04$ in order to place the emission altitude near the mesopause where the temperature is ∼ 135 K. This is difficult to understand in light of the results shown in Fig. 7. and no details were presented by Geballe et al. (2003) to support their temperature determination. The large HCN mole fraction near 600 km determined by Geballe et al. (2003) is a consequence of the large value adopted for P_{10}. Figure 6 shows a curve of growth for a model similar to that of Geballe et al. (2003), along with the single scattering albedo corresponding to $P_{10} = 0.1$. The calculations use an HCN mole fraction of 0.01 at pressures less than 1 μbar and the Marten et al. (2002) results at higher pressure. The large values of P_{10} and X_∞(HCN) in the Geballe et al. (2003) model imply that the amount of flux is absorbed is similar to that in our baseline model. In fact, our calculations of a synthetic spectrum using these model parameters agrees well with the Geballe et al. calculations. The difference then concerns only the temperature sensitivity. We find that the spectrum is insensitive to temperature changes of tens of Kelvins and that, if anything, the observations are better matched by a temperature higher than that in the baseline model. Geballe et al. (2003) claim that the spectrum is highly sensitive to temperature and that most of the scattering must take place near the mesopause in order to reproduce the low rotational temperature inferred from the observations.
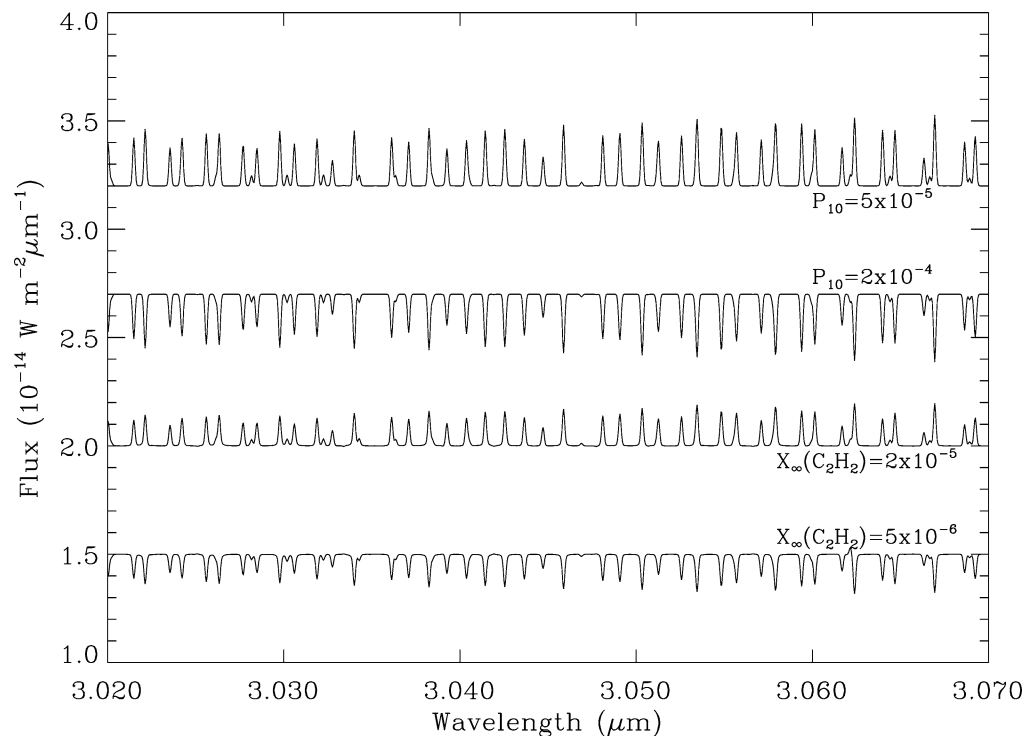
Fig. 8. Sensitivity tests for C_2H_2 model parameters. The curves show the difference between the modified models and the baseline model. Only one parameter is modified at a time and the varied parameter is listed next to the curve.

We have also explored the sensitivity of the model spectra to C_2H_2 model parameters (Fig. 8). Interestingly, the spectrum is more sensitive to the abundance of C_2H_2 in the thermosphere than was the case for HCN. Holding P_{10} fixed, we calculate that more than a factor of 2 increase in $X_\infty(C_2H_2)$ would produce more C_2H_2 fluorescence than observed. This is most apparent at 3.058 and 3.0625 μm. A value of $X_\infty(C_2H_2)$ a factor of two smaller causes the absorption lines to be too deep. Similarly, assuming our baseline model for the C_2H_2 distribution, we calculate that a factor of 2 variation of P_{10} in either direction degrades the match between synthetic and observed spectra.

5. Summary

We have shown that the HCN emissions arise primarily from scattering in Titan's middle atmosphere at pressures near 1 mbar. A good match to the observed spectrum is achieved with a model that incorporates the HCN distribution of Marten et al. (2002), the thermal profile of Yelle et al. (1997), and collisional de-excitation rates a factor of ten lower than the room temperature values measured in the laboratory (Hastings et al., 1983). The HCN mole fraction in the thermosphere cannot be accurately inferred from the ν_3 band observations. Models that have mole fractions in the thermosphere from 3×10^{-3} to 10^{-5} fit the observations equally well. We also find that the spectrum is insensitive to temperature variations of tens of kelvins. Thus, the band formation region cannot be determined using relative rotational line strengths. This result differs from that presented by Geballe et al. (2003) who argued that the spectrum could only be matched by HCN emissions that arose near the mesopause. We conclude that there is no evidence for the HCN densities greatly in excess of currently accepted values, as suggested by Geballe et al. (2003). Nor do we require collisional de-excitation rates greatly in excess of laboratory measurements to explain the observations.

The lack of C_2H_2 emission features requires a low abundance of C_2H_2 in Titan's thermosphere. Our analysis establishes an upper limit to the mole fraction of 10^{-5} for $P_{10} = 10^{-4}$. This upper limit is lower if P_{10} decreases with temperature. Photochemical models of Yung et al. (1984), Toublanc et al. (1995), and Lara et al. (1996) predict $X_\infty(C_2H_2)$ values of 10^{-2}, 2×10^{-3}, and 10^{-3}, respectively. It appears that $X_\infty(C_2H_2)$ is lower than photochemical predictions as long as P_{10} at Titan temperatures is equal to or lower than its room temperature value. Potentially, this is an important spectral region for determining C_2H_2 mole fraction because it constrains the abundance in the thermosphere where C_2H_2 is created. The C_2H_2 ν_3 spectrum therefore constrains the photochemical models in a region that is not strongly affected by uncertain atmospheric mixing rates. Our results are consistent with the Vervack (1997) analysis of the Voyager UVS occultation observations and can be further tested with Cassini observations.

Observations with a higher signal-to-noise ratio and less contamination by telluric absorption might place useful constraints on the temperature in Titan's atmosphere. In the past, the temperature in Titan's middle atmosphere has been stud-

ied with space-based observations of the CH_4 ν_4 band. Inference of the temperature through HCN observations would complement the CH_4 studies and might provide a useful way to monitor temperature from groundbased observatories.

The temperature dependence of the collisional de-excitation rates is the primary uncertainty in our analysis. The analytic approximations to P_{10} in common use (Landau and Teller, 1936; Schwartz et al., 1952) predict that P_{10} decreases with decreasing temperature (Yelle, 1991); however, these approaches were developed for V–T reactions while it appears that the ν_3 states of both HCN and C_2H_2 are de-excited by V–V reactions. Further laboratory studies of these processes would enhance the value of observations of fluorescence in the C–H stretch modes of hydrocarbons in planetary atmospheres.

Acknowledgment

Appendix A

Inspection of the spectrum shown in Fig. 1 reveals significant overlap between the HCN emission and C_2H_2 absorption lines. We therefore derive a radiative transfer equation that incorporates overlap of two vibrational bands assuming rotational LTE. The formulation is an extension of that described by Yelle (1991). We write the absorption coefficient as

$$k_\nu = k_\nu^A + k_\nu^B, \tag{A.1}$$

where the superscripts A and B denote the bands. The emission coefficient is

$$
\begin{aligned}
j_\nu = {} & \frac{B_\nu}{B^A} \frac{k_\nu^A}{k^A} \int_{\text{band}} k_\nu^A \left(\overline{w}^A \left(J_\nu + \frac{F_\nu}{4\pi} e^{-\tau_\nu/\mu_\circ} \right) \right. \\
& \left. + \left(1 - \overline{w}^A\right) B_\nu \right) d\nu \\
& + \frac{B_\nu}{B^B} \frac{k_\nu^B}{k^B} \int_{\text{band}} k_\nu^B \left(\overline{w}^B \left(J_\nu + \frac{F_\nu}{4\pi} e^{-\tau_\nu/\mu_\circ} \right) \right. \\
& \left. + \left(1 - \overline{w}^B\right) B_\nu \right) d\nu, \tag{A.2}
\end{aligned}
$$

where J_ν is the mean intensity, F_ν is the solar flux at solar zenith angle $\cos^{-1}(\mu_\circ)$, and B_ν is the Planck function. The single scattering albedo for the band is given by

$$\overline{w}^{A,B} = \frac{A_{10}^{A,B}}{A_{10}^{A,B} + C_{10}^{A,B}}, \tag{A.3}$$

where $A_{10}^{A,B}$ and $C_{10}^{A,B}$ are the radiative and collisional de-excitation rates for the upper vibrational states of the bands.

Variables without the ν subscript are band averages,

$$k^{A,B} = \int_{\text{band}} k_\nu^{A,B} \, d\nu, \qquad B^{A,B} = \int_{\text{band}} \frac{k_\nu^{A,B}}{k^{A,B}} B_\nu \, d\nu. \tag{A.4}$$

The source function is given by

$$S_\nu = S_\nu^\circ + U_\nu^A J^A + U_\nu^B J^B, \tag{A.5}$$

where

$$
\begin{aligned}
S_\nu^\circ = {} & (1 - \overline{w}_\nu) B_\nu + U_\nu^A \int_{\text{band}} w_\nu^A \frac{F_\nu e^{-\tau_\nu/\mu_\circ}}{4\pi} \, d\nu \\
& + U_\nu^B \int_{\text{band}} w_\nu^B \frac{F_\nu e^{-\tau_\nu/\mu_\circ}}{4\pi} \, d\nu, \tag{A.6}
\end{aligned}
$$

$$U_\nu^{A,B} = \overline{w}^{A,B} p_\nu^{A,B} \frac{B_\nu}{B^{A,B}}, \tag{A.7}$$

$$w_\nu^{A,B} = \frac{k_\nu^{A,B}}{k^{A,B}}, \qquad p_\nu^{A,B} = \frac{k_\nu^{A,B}}{k_\nu^A + k_\nu^B}, \tag{A.8}$$

and

$$\overline{w}_\nu = p_\nu^A \overline{w}^A + p_\nu^B \overline{w}^B. \tag{A.9}$$

The mean intensities and source functions for each band are defined as

$$J^{A,B} = \int_{\text{band}} w_\nu^{A,B} J_\nu \, d\nu, \tag{A.10}$$

and

$$S^{A,B} = \int_{\text{band}} w_\nu^{A,B} S_\nu \, d\nu. \tag{A.11}$$

To solve this system of equations we write the radiative transfer equation in the Feautrier form

$$\mu^2 \frac{\partial^2 u_\nu}{\partial \tau_\nu^2} = u_\nu - S_\nu, \tag{A.12}$$

where $u_\nu(\mu) = \frac{1}{2}(I_\nu(+\mu) + I_\nu(-\mu))$. Substituting the expression for the source function and rearranging terms we have

$$u_\nu - \mu^2 \frac{\partial^2 u_\nu}{\partial \tau_\nu^2} = S_\nu^\circ + U_\nu^A J^A + U_\nu^B J^B. \tag{A.13}$$

We now switch notation and use bold symbols to denote vectors and matrices containing the depth variation of the variables and the subscript i to denote a frequency-angle point. The radiative transfer equation becomes

$$\mathbf{T}_i \cdot \mathbf{u}_j = \mathbf{S}_i^\circ + \mathbf{U}_i^A \cdot \mathbf{J}^A + \mathbf{U}_i^B \cdot \mathbf{J}^B, \tag{A.14}$$

where $\mathbf{T}_i$ represents $1 - \mu^2 \partial^2/\partial \tau_\nu^2$, $\mathbf{U}_i^{A,B}$ is a diagonal matrix containing the values of $U_\nu^{A,B}$ and $\mathbf{S}_i^\circ$ is a vector containing the values of S_ν°. The mean intensities are related to

the Feautrier variables through

$$\mathbf{J}^{A,B} = \sum_i \mathbf{w}_i^{A,B} \mathbf{u}_i, \tag{A.15}$$

where $\mathbf{w}_i$ is a diagonal matrix containing the weights for the integration over frequency and angle. Eliminating $\mathbf{u}_i$ from Eq. (A.14), we obtain two coupled equations for the mean intensity

$$\left(\mathbf{1} - \sum_i \mathbf{w}_i^A \mathbf{T}_i^{-1} \mathbf{U}_i^A \right) \mathbf{J}^A$$

$$= \left(\sum_i \mathbf{w}_i^A \mathbf{T}_i^{-1} \mathbf{U}_i^B \right) \mathbf{J}^B + \sum_i \mathbf{w}_i^A \mathbf{T}_i^{-1} \mathbf{S}_i^\circ,$$

$$\left(\mathbf{1} - \sum_i \mathbf{w}_i^B \mathbf{T}_i^{-1} \mathbf{U}_i^B \right) \mathbf{J}^B$$

$$= \left(\sum_i \mathbf{w}_i^B \mathbf{T}_i^{-1} \mathbf{U}_i^A \right) \mathbf{J}^A + \sum_i \mathbf{w}_i^B \mathbf{T}_i^{-1} \mathbf{S}_i^\circ. \tag{A.16}$$

We now define

$$\mathbf{M}^{A,B} = \mathbf{1} - \sum_i \mathbf{w}_i^{A,B} \mathbf{T}_i^{-1} \mathbf{U}_i^{A,B}, \tag{A.17}$$

$$\mathbf{N}^{AB,BA} = \sum_i \mathbf{w}_i^{A,B} \mathbf{T}_i^{-1} \mathbf{U}_i^{B,A}, \tag{A.18}$$

and

$$\mathbf{L}^{A,B} = \sum_i \mathbf{w}_i^{A,B} \mathbf{T}_i^{-1} \mathbf{S}_i^\circ. \tag{A.19}$$

The coupled equations become

$$\mathbf{M}^A \mathbf{J}^A = \mathbf{N}^{AB} \mathbf{J}^B + \mathbf{L}^A, \tag{A.20}$$

$$\mathbf{M}^B \mathbf{J}^B = \mathbf{N}^{BA} \mathbf{J}^A + \mathbf{L}^B, \tag{A.21}$$

where the $\mathbf{N}^{AB}$ matrices represent the coupling between the bands. $\mathbf{N}^{AB}$ is significant if k_ν^A and k_ν^B are correlated. In the limit of no overlap equations (A.20) and (A.21) reduce to the expression for independent bands. The solution to Eqs. (A.20) and (A.21) is

$$\mathbf{J}^A = \left(\mathbf{1} - \left(\mathbf{M}^A \right)^{-1} \mathbf{N}^{AB} \left(\mathbf{M}^B \right)^{-1} \mathbf{N}^{BA} \right)^{-1} \left(\mathbf{M}^A \right)^{-1}$$

$$\times \left(\mathbf{N}^{AB} \left(\mathbf{M}^B \right)^{-1} \mathbf{L}^B + \mathbf{L}^A \right), \tag{A.22}$$

$$\mathbf{J}^B = \left(\mathbf{1} - \left(\mathbf{M}^B \right)^{-1} \mathbf{N}^{BA} \left(\mathbf{M}^A \right)^{-1} \mathbf{N}^{AB} \right)^{-1} \left(\mathbf{M}^B \right)^{-1}$$

$$\times \left(\mathbf{N}^{BA} \left(\mathbf{M}^A \right)^{-1} \mathbf{L}^A + \mathbf{L}^B \right). \tag{A.23}$$

References

Coustenis, A., Bézard, B., Gautier, D., 1995. Titan's atmosphere from Voyager infrared observations, IV. Latitudinal variations of temperatures and composition. Icarus 115, 126–140.

Coustenis, A., Salama, A., Schultz, B., Ott, S., Lellouch, E., Encrenaz, Th., Gautier, D., Feuchtgruber, H., 2003. Titan's atmosphere from ISO mid-infrared spectroscopy. Icarus. In press.

Dinelli, B.M., Miller, S., Achilleos, N., Lam, H.A., Cahill, M., Tennyson, J., Jagod, M.F., Oka, T., Hilico, J.-C., Geballe, T.R., 1997. UKIRT observations of the impact and consequences of Comet Shoemaker–Levy 9 on Jupiter. Icarus 126, 107–125.

Drossart, P., Fouchet, Th., Crovisier, J., Lellouch, E., Encrenaz, Th., Feuchtgruber, F., Champion, J.-P., 1998. Fluorescence in the 3 micron bands of methane on Jupiter and Saturn from ISO/SWS observations. In: Proceedings of the Conference "The Universe as Seen by ISO." In: ESA SP, Vol. 427.

Geballe, T.R., Kim, S.J., Noll, K.S., Griffith, C.A., 2003. High-resolution 3 micron spectroscopy of molecules in the mesosphere and troposphere of Titan. Astrophys. J. 583, L39.

Griffith, C.A., Owen, T., Miller, G.A., Geballe, T.R., 1998. Transient clouds in Titan's lower atmosphere. Nature 395, 575–579.

Hager, J., Krieger, W., Pfab, J., 1980. Collisional deactivation of laser-excited acetylene by H_2, HBr, N_2 and CO. J. Chem. Soc. Faraday Trans. 2 77, 477–493.

Hastings, P.W., Osborn, M.K., Sadowski, C.M., Smith, I.W.M., 1983. Vibrational relaxation of $HCN(002)^{a)}$. J. Chem. Phys. 78, 3893–3898.

Jacquinet-Husson, N., 19 colleagues, 1999. The 1997 spectroscopic GEISA databank. J. Quant. Spectrosc. Radiat. Transfer, 205–254.

Kim, S.J., Orton, G.S., Dumas, C., Kim, Y.H., 1996. Infrared spectroscopy of Jupiter's atmosphere after the A and E impacts of Comet Shoemaker–Levy 9. Icarus 120, 326–332.

Kim, S.J., Geballe, T.R., Noll, K.S., 2000. Three-micrometer CH_4 line emission from Titan's high-altitude atmosphere. Icarus 147, 588–591.

Lambert, J.D., 1977. Vibrational and Rotational Relaxation in Gases. Clarendon Press, Oxford, New York.

Landau, L., Teller, E., 1936. Theory of sound dispersion. Phys. Z. 10, 34.

Lara, L.M., Lellouch, E., Lopez-Moreno, J.J., Rodrigo, R., 1996. Vertical distribution of Titan's atmospheric neutral constituents. J. Geophys. Res. 101, 23261–23283.

Lindal, G.F., Wood, G.E., Holz, H.B., Sweetnam, D.N., Eshleman, V.R., Tyler, G.L., 1983. The atmosphere of Titan: an analysis of the Voyager 1 radio-occultation measurements. Icarus 53, 348–363.

Lellouch, E., Hunten, D.M., Kockarts, G., Coustenis, A., 1990. Titan's thermosphere profile. Icarus 83, 308–324.

Marten, A., Hidayat, T., Biraud, Y., Moreno, R., 2002. New millimeter heterodyne observations of Titan: vertical distributions of nitriles HCN, HC_3N, CH_3CN and the isotopic ratio $^{14}N/^{14}N$ in its atmosphere. Icarus 158, 532–544.

Schwartz, R.N., Slawsky, Z.I., Herzfeld, K.F., 1952. Calculation of vibrational relaxation times in gases. J. Chem. Phys. 20, 1591–1599.

Smith, G.R., Strobel, D.F., Broadfoot, A.L., Sandel, B.R., Shemansky, D.E., Holberg, J.B., 1983. Titan's upper atmosphere—composition and temperature from the EUV solar occultation results. J. Geophys. Res. 87, 1351–1359.

Toublanc, D., Parisot, J.P., Brillet, J., Gautier, D., Raulin, F., McKay, C.P., 1995. Photochemical modeling of Titan's atmosphere. Icarus 113, 2–16.

Weaver, H.A., Chin, G., Fox, K., 1989. Methane fluorescence in comets. Bull. Am. Astron. Soc. 21, 937.

Yelle, R.V., 1991. Non-LTE models of Titan's upper atmosphere. Astrophys. J. 383, 380–400.

Yelle, R.V., Strobel, D.F., Lellouch, E., Gautier, D., 1997. Engineering models for Titan's atmosphere. In: Huygens Science, Payload, and Mission. In: ESA SP, Vol. 1177. Estec Publications Division, ESTEC, Noordwijk, The Netherlands.

Yung, Y.L., Allen, M., Pinto, J.P., 1984. Photochemistry of the atmosphere of Titan: comparison between model and observations. Astrophys. J. Suppl. 55, 465–506.

Vervack Jr., R.J., 1997. Titan's upper atmospheric structure derived from Voyager Ultraviolet Spectrometer Observations. PhD Dissertation. The University of Arizona, Tucson, AZ.